Oxygen desorption properties of perovskite-type $SrFe_{1-x}Co_xO_{3-\delta}$: *B*-site mixing effect on the reduction properties of Fe and Co ions

Fumito Fujishiro[1], Natsumi Oshima[1], Tokio Sakuragi[2], and Masatsugu Oishi[2]

[1]Faculty of Science and Technology, Kochi University, 2-5-1 Akebono-cho, Kochi-shi, Kochi, 780-8520, Japan

[2]Graduate School of Technology, Industrial and Social Science, Tokushima University, 2-1 Minami Josanjima, Tokushima-shi, Tokushima, 770-8506, Japan

Corresponding author

Fumito Fujishiro, f.fujishiro@kochi-u.ac.jp

Abstract

To understand the *B*-site mixing effect in perovskite-type $SrFe_{1-x}Co_xO_{3-\delta}$, we evaluated the relationship between the oxygen desorption properties and the reduction behavior of Fe and Co ions using thermogravimetry and in-situ X-ray absorption spectroscopy. The valence states of Fe and Co ions were estimated to be 3.56+ and 3.27+, respectively, which remained constant with changes in composition. Maximum oxygen desorption occurred at $x = 0.2$ below 800 °C. As temperature was increased and oxygen was released, a relationship was observed between the valence and coordination number changes of each *B*-site ion; these changes were more pronounced for the Fe ions than for the Co ions. In $SrFe_{1-x}Co_xO_{3-\delta}$ samples, oxygen adjacent to Fe ions was released more readily than oxygen adjacent to Co ions. This conclusion is supported by the electronic states of the two *B*-site ions. These results are important for the design of new oxygen storage materials.

Keywords: Oxygen storage materials, Perovskite-type oxides, B-site mixing effect, Thermogravimetry, X-ray absorption spectroscopy

1. Introduction

Oxygen storage materials (OSMs) are important functional ceramics that utilize gas-solid reactions: redox reactions of constituent transition metals lead to reversible oxygen sorption/desorption. These redox reactions are triggered by changes in the partial oxygen pressure of the surrounding atmosphere and/or by changes in temperature. OSMs have been used in various applications such as oxygen-permeable membranes for H_2 production [1,2] and chemical looping [3–5].

Among the numerous oxide candidates for OSMs, perovskite-type ABO_3 oxides have attracted considerable attention because their electronic, structural, and thermodynamic properties are readily tuned by substitution at the *B*-site. In particular, $SrFeO_{3-\delta}$-based solid solutions have been considered for the development of new OSMs. Demizu *et al.* reported that $SrFe_{1-x}Ti_xO_{3-\delta}$ exhibits higher oxygen intake/release rates in the presence of CO_2 than un-doped $SrFeO_{3-\delta}$ [6]. $SrFe_{1-x}Mn_xO_{3-\delta}$ was found to possess a capability for oxygen storage during temperature changes in air due to the redox behavior of Fe ions [7]. Although Mn is a transition metal, the valence state of Mn ions in $SrFe_{1-x}Mn_xO_{3-\delta}$ is stable during oxygen sorption/desorption; this is in contrast to the redox behavior of Mn ions in $Ca_2AlMnO_{5+\delta}$ in the presence of O_2 [8]. Kusaba *et al*. reported that $SrFe_{1-x}Co_xO_{3-\delta}$ exhibits an enhanced oxygen storage capacity when

experiencing temperature changes in air [9]. The unique characteristics mentioned here are attributed to the coexistence of two *B*-site ions, i.e. the *B*-site mixing effect. Investigating the valence and local atomic structural changes of each individual *B*-site ion during oxygen desorption is important to gain a detailed understanding of this effect. In addition, such an investigation should be performed for samples composed of a wide range of *B*-site ions.

Cobalt is a neighbor of iron on the periodic table, opposite to manganese, and the ionic radii of its trivalent and tetravalent ions are closer to those for iron compared to those for manganese. Due to this, Co-doped $SrFe_{1-x}Co_xO_{3-\delta}$ exhibits a wider composition range ($x \leq 0.8$) than $SrFe_{1-x}Mn_xO_{3-\delta}$ ($x \leq 0.6$) [7,9]. In this study, the relationship between the oxygen desorption properties and reduction behavior for both Co and Fe ions in *B*-site mixed $SrFe_{1-x}Co_xO_{3-\delta}$ was evaluated using thermogravimetry, iodometry, and X-ray absorption spectroscopy (XAS). In addition, the influence of the reduction of each *B*-site ion on oxygen desorption was investigated.

2. Experimental

$SrFe_{1-x}Co_xO_{3-\delta}$ samples were prepared using the Pechini method. $SrCO_3$ (99.9%, Wako), $Fe(NO_3)_3 \cdot 9H_2O$ (99.4%, Wako), and $Co(NO_3)_2 \cdot 6H_2O$ (99.4%, Wako) were used

as starting materials. The purity of the nitrides was determined using the ignition loss technique. The detailed procedures used in this study have been discussed in our previous paper [10]. Heating in air at 1200 °C yielded $SrFe_{1-x}Co_xO_{3-\delta}$. The crystal structures of the obtained samples were characterized by X-ray diffraction (XRD) using Cu Kα radiation (40 kV, 40 mA, RINT2200; Rigaku Co., Ltd., Japan). Thermogravimetry–differential thermal analysis (TG–DTA) was performed in air at a heating/cooling rate of 10 °C/min from room temperature to 1000 °C; the measurement was subsequently performed three times to confirm reversibility. XAS measurements of the Fe and Co *K*-edges were performed using beamline BL01B1 at SPring-8 (Hyogo, Japan) [11]. *In-situ* XAS measurements of the sample with $x = 0.4$ were performed in air at 700 °C, and the procedure was similar to that previously reported by our group [12]. The X-ray absorption fine structure spectra were recorded in the transmission mode using ionization chamber detectors and analyzed with Demeter software [13].

3. Results and discussion

3.1. Characterization of $SrFe_{1-x}Co_xO_{3-\delta}$

Figure 1 shows the XRD patterns of $SrFe_{1-x}Co_xO_{3-\delta}$ with $0 \leq x \leq 0.8$. The pattern of $SrFeO_{3-\delta}$ ($x = 0$) was assigned to an orthorhombic $Sr_4Fe_4O_{11}$-type structure (*Cmmm*,

no. 65) [14], and the same phase was identified for the sample with $x = 0.2$. The patterns of samples with $0.4 \leq x \leq 0.8$ were assigned to a cubic perovskite-type structure ($Pm\bar{3}m$, no. 221), though some trace peaks with diamond symbols could be assigned to tetragonal $SrCoO_{2.87}$ ($I4/mmm$, no. 139) [15]. The low intensity of these trace peaks indicated a negligible amount of the $SrCoO_{2.87}$ phase; thus, the influence of this second phase on oxygen desorption properties is ignored. Molar volumes estimated using the XRD patterns remained constant with changing Co content (Fig. S1), although the ionic radii of trivalent and tetravalent Fe ions are larger than those of the Co ions in the same valence state. This feature suggests that mixed valence states were obtained for the Fe and Co ions in the samples, because the ionic radius of Fe^{4+} (0.585 Å) is smaller than that of Co^{3+} (0.61 Å) in the six-fold coordination [16].

The normalized X-ray absorption near-edge structure (XANES) spectra of the $SrFe_{1-x}Co_xO_{3-\delta}$ samples are shown in Fig. 2. Figure 2(a) shows the Fe *K*-edge XANES spectra of the obtained samples, as well as the XANES spectra of a brownmillerite-type $Sr_2Fe_2O_5$ that was prepared using the Pechini method by heating in N_2 at 1200 °C, as a reference for Fe^{3+}. Figure 2(b) displays the Co *K*-edge spectra of the samples with $0.2 \leq x \leq 0.8$. The XANES spectra of a rock-salt-type CoO (Co^{2+}) and rhombohedral perovskite-type $LaCoO_3$ (Co^{3+}) are also shown in Fig. 2(b) as references. The $LaCoO_3$

sample was prepared using the same Pechini method by heating in air at 900 °C, and its crystal structure was characterized by XRD as the rhombohedral perovskite-type with space group $R\bar{3}c$ (no. 167) [17]. As shown in Fig. 2(a), the Fe *K*-edge absorption energies of the obtained samples were all higher than that of Fe^{3+} in $Sr_2Fe_2O_5$; the Fe *K*-edge absorption energy remained constant with a change in the Co content. The Co *K*-edge absorption energies of the obtained samples were all somewhat close to that of Co^{3+} in $LaCoO_3$, and edge shapes were unaffected by the Co content (Fig. 2(b)). These unchanged absorption edge energies indicate that the valence states of both *B*-site ions are independent of the composition, which is also the case for $SrFe_{1-x}Mn_xO_{3-\delta}$.

Table 1 lists the results of iodometry for the obtained samples. The Fe valence of $SrFeO_{3-\delta}$ (x = 0) was 3.56+, and the average valence of the *B*-site ions decreased with increasing Co content. For the solid solutions, the valence was calculated when both Fe and Co were reduced to divalent ions in an acidic solution with excess KI as the reducing agent. The oxygen (3−δ) and vacancy (δ) contents were estimated using the electrically neutral conditions represented in Equation (1) below, assuming Sr and O valences of 2+ and 2−, respectively:

$$1 \times (2+) + 1 \times (\text{average } B \text{ valence}) + (3-\delta) \times (2-) = 0 \quad (1).$$

Based on the results of the XANES spectra in Fig. 2, the Fe valence in the obtained

samples was unchanged as 3.56+. Assuming that the Co valence was 3.27+, the average *B* valence was estimated using Equation (2) below:

average *B* valence = (3.56+) × (1−*x*) (Fe content) + (3.27+) × *x* (Co content) (2).

These results are presented in Table 1. The estimated average values were in good agreement with those obtained by iodometry, and therefore, the valence states of the Fe and Co ions in the $SrFe_{1-x}Co_xO_{3-\delta}$ samples were determined as constant values of 3.56+ and 3.27+, respectively.

3.2 Oxygen desorption of $SrFe_{1-x}Co_xO_{3-\delta}$

Figure 3 shows the weight change Δw of the $SrFe_{1-x}Co_xO_{3-\delta}$ samples in air. As the temperature increased above approximately 400 °C, all samples showed a weight loss due to oxygen desorption; a reversible weight change occurred by then cooling in air, as shown in the inset. The onset temperatures, as indicated by the two vertical arrows above the TG curves, first decreased due to Co-doping from 385 °C to 356 °C (for $x = 0.2$), and then increased to 371 °C (for $x = 0.8$). Jia *et al*. reported the density functional theory (DFT) calculations for the Co-doping effect on oxygen vacancy formation in $SrFe_{1-x}Co_xO_{3-\delta}$; the results indicated that the formation energy of oxygen vacancies (ΔE_f) decreases with increasing Co content of $SrFe_{1-x}Co_xO_{3-\delta}$ with a constant oxygen

nonstoichiometry [18]. This decrease in ΔE_f allows for easy oxygen desorption from the crystal lattice, resulting in weight loss due to oxygen desorption at lower temperatures. This may explain the decrease in the onset temperature for the sample with x = 0.2 compared with that of $SrFeO_{3-\delta}$ (x = 0), because the amounts of vacancies in these samples were similar (Table 1). In addition, the DFT calculations indicated that an increase in vacancies enhances ΔE_f; this is also reported for the same perovskite-type $Sr_{0.8}Ca_{0.2}FeO_3$ and $Sr_{0.8}Ca_{0.2}Fe_{0.4}Co_{0.6}O_3$ [19]. Therefore, the increase in onset temperature observed between the samples with x = 0.2 and x = 0.8 may be explained the increase in vacancy content (see Table 1). Another possibility that could explain the changes in the onset temperature is the difference in the oxygen desorption rate because thermal behaviors at low temperatures are governed by kinetics as well as thermodynamics. The dependence of the oxygen desorption rate on Fe and Co composition could also vary the onset temperature.

The oxygen desorption amount ($\Delta\delta$) was calculated from Δw using Equation (3):

$$\Delta\delta = |\Delta w| \cdot \frac{M_S}{M_O} \quad (3),$$

where M_S and M_O represent the molar mass of the obtained samples by considering oxygen nonstoichiometry and the atomic mass of oxygen, respectively. Figure 4 shows a plot of $\Delta\delta$ vs. Co content. The maximum change in $\Delta\delta$ at lower temperatures occurred at

x = 0.2; this is largely attributed to the change in onset temperature (Fig. 3). At higher temperatures, however, the Δδ value decreased monotonously with increasing Co content. The pre-edge peaks and absorption edge in the Fe and Co *K*-edge XANES spectra of $SrFe_{0.6}Co_{0.4}O_{3-\delta}$ samples shifted towards lower energies when the samples were heated in air, indicating that both Fe and Co ions were reduced due to oxygen desorption (Fig. S2 (a) and (b)). As described earlier, the valence state of the Fe ions (3.56+) was higher than that of the Co ions (3.27+). Thus, assuming that Fe and Co ions were both reduced to a trivalent state at high temperatures, an increase in the Co content would reduce Δδ, as observed in Fig. 4. In contrast, $SrFe_{1-x}Mn_xO_{3-\delta}$ samples including $Fe^{3.56+}$ and Mn^{4+} showed a monotonous decrease in Δδ with increasing Mn content; in this case, it was concluded that oxygen absorption arises only from the reduction of Fe ions [7]. As an additional point, no thermal events due to phase transitions were observed in any of the DTA curves. This indicated that all $SrFe_{1-x}Co_xO_{3-\delta}$ samples maintained their crystal structure during oxygen desorption. Such structural stability during oxygen release in air is similar to the behavior described for $SrFe_{1-x}Mn_xO_{3-\delta}$ [7].

Local atomic structural changes around the Fe and Co ions due to oxygen desorption were observed *via* k^3-weighted extended X-ray absorption fine structure (EXAFS) oscillations (Fig. S2 (c) and (d)). Figure 5 shows the amplitude of Fourier

transforms of the obtained EXAFS oscillations in a *k* space of 3–11 Å, |□(R)|, for $SrFe_{0.6}Co_{0.4}O_{3-\delta}$ at room temperature and at 700 °C. The results for Fe and Co ions are shown in Fig. 5(a) and (b), respectively. A peak with a shoulder at ~1.5 Å and two combined peaks located between 2.5 and 4.0 Å were observed on the |□(R)| for both ions at room temperature. Our previous study on EXAFS oscillations of perovskite-type $SrFeO_{3-\delta}$ revealed that the first peak corresponds to the Fe–O correlation in the $FeO_{6-\delta}$ polyhedron, whereas the other peaks are attributed to the second and third coordination shell by Fe–Sr and Fe–Fe, respectively [12]. Accordingly, the obtained peaks were assigned, as shown in Fig. 5. When the temperature was increased, the intensities of the obtained peaks decreased due to an increase in Debye–Waller factors; the second and third peaks were hardly observed at 700 °C. The decrease in intensity of the Fe–O correlation was more pronounced than that of the Co–O correlation, which indicated a larger decrease in coordination number for Fe ions than for Co ions. As mentioned previously, the valence change due to reduction is larger for the Fe ions than for the Co ions; therefore, these results suggested that oxygen adjacent to the Fe ions was easily released. The d-level electronic configurations of Co ions are represented as d^6 for Co^{3+} and d^5 for Co^{4+}. Potze et al. reported that the spin states of Co ions with the d^5 and d^6 configurations can adopt an intermediate spin state in perovskite-type $SrCoO_3$ and

$LaCoO_3$ [20]. Magnetic measurements of $SrFe_{1-x}Co_xO_{3-\delta}$ indicated the existence of Co ions with a low spin state as well as an intermediate spin state [21,22]. However, lanthanoid-containing perovskite-type cobalt oxides showed an insulator–metal transition at approximately 350 °C, which suggested that a spin transition from the intermediate spin state to a high spin state occurred [23]. Because the obtained $SrFe_{1-x}Co_xO_{3-\delta}$ samples show oxygen desorption at temperatures above 400 °C, the Co ions in the samples exhibit high spin states during reduction. In contrast, the electronic state of Fe^{3+} is a d^5 configuration with a high spin state, and that of Fe^{4+} in the cubic perovskite-type $SrFeO_{3-\delta}$ is denoted as a $d^5\underline{L}$ (where $\underline{L}$ refers to a ligand hole) configuration rather than a d^4 configuration [24]. This Fe^{4+} can also be represented as Fe^{3+} + $h^{\bullet}$. When oxygen desorption occurs, two electrons remain in the crystal lattice, as represented in Equation (4):

$$O_O^{\times} \rightarrow V_O^{\cdot\cdot} + 2e' + \frac{1}{2}O_2$$

where the notation follows the Kröger-Vink notation. During reduction, Co^{4+} traps the generated electron to create one electron pair at a *d*-orbital, resulting in d^6 configuration. In contrast, Fe^{4+} is reduced simply by combining the generated electron with the ligand hole $h^{\bullet}$ by Fe^{3+}. The results of our previous study revealed that the cubic perovskite-type $SrFe_{1-x}Mn_xO_{3-\delta}$ displays reversible oxygen sorption/desorption due to the redox reaction

of Fe ions only; Mn^{4+} is not reduced because the Jahn–Tellar Mn^{3+} is unstable in the cubic symmetry [7]. The electronic configurations of Mn, Fe, and Co ions in the cubic perovskite-type $SrFe_{1-x}M_xO_{3-\delta}$ (M = Mn, Co) are shown in Fig. 6. Comparing the reduction pathways between these ions, Fe ions receive an electron that combines with a ligand hole by Coulomb interaction, Co ions adopt d^6 configuration with one electron pair, and Mn ions, if possible, become Jahn–Tellar ions with d^4 configuration. Such differences in reduction behavior produced the site-selective oxygen release observed in the *B*-site mixed $SrFe_{1-x}Co_xO_{3-\delta}$ samples.

4. Conclusions

The results of this study indicated several important factors governing the oxygen absorption/desorption properties of *B*-site mixed perovskite-type $SrFe_{1-x}Co_xO_{3-\delta}$: changes in the onset temperature due to changes in composition, the relationship between the electronic state and reducibility of each ion species, and the ease of oxygen release by Fe ions. The valence state of Fe was found to be greater than that of Co, and both values remained constant irrespective of the Co content. The doping of Co into the Fe sites of $SrFe_{1-x}Co_xO_{3-\delta}$ reduced the onset temperature of oxygen desorption, and this, in turn, enhanced $\Delta\delta$ at lower temperatures. The electronic states of the *B*-site ions determined

their reducibility during oxygen desorption, and the difference in reducibility indicated that desorption of oxygen adjacent to Fe ions occurs more readily than for oxygen adjacent to Co ions in $SrFe_{1-x}Co_xO_{3-\delta}$. Thus, these findings play an important role in understanding the *B*-site mixing effects; this is essential for the design of new OSMs, and will facilitate the preparation of other oxides with superior properties currently under consideration.

Author Contributions

Fumito Fujishiro: Conceptualization, Funding acquisition, Investigation, Project administration, Resources, Visualization, Writing - original draft

Natsumi Oshima: Investigation, Visualization

Tokio Sakuragi: Investigation

Masatsugu Oishi: Investigation, Resources, Visualization, Writing - review & editing

Acknowledgements

The authors thank Dr. Toshiaki Ina, JASRI SPring-8, for his excellent technical support in X-ray absorption spectroscopy. This work was supported by a Grant-in-Aid for Science Research (Grant Number JP 18K05276) from the Japan Society for the

Promotion of Science. The XAS experiments in this study were conducted at SPring-8 under proposals 2017B1437, 2018A1174, 2018B1446, and 2019B1146.

References

[1] H. Takamura, K. Enomoto, Y. Aizumi, A. Kamegawa, M. Okada, Preparation and oxygen permeability of Pr–Al-based perovskite-type oxides, Solid State Ionics. 175 (2004) 379–382. https://doi.org/10.1016/j.ssi.2004.02.080.

[2] Y. Hayamizu, M. Kato, H. Takamura, Effects of surface modification on the oxygen permeation of $Ba_{0.5}Sr_{0.5}Co_{0.8}Fe_{0.2}O_{3-\delta}$ membrane, J. Membr. Sci. 462 (2014) 147–152. https://doi.org/10.1016/j.memsci.2014.03.038.

[3] L. Nalbandian, A. Evdou, V. Zaspalis, $La_{1-x}Sr_xM_yFe_{1-y}O_{3-\delta}$ perovskites as oxygen-carrier materials for chemical-looping reforming, Int. J. Hydr. Energy. 36 (2011) 6657–6670. https://doi.org/10.1016/j.ijhydene.2011.02.146.

[4] J. Vieten, B. Bulfin, F. Call, M. Lange, M. Schmücker, A. Francke, M. Roeb, C. Sattler, Perovskite oxides for application in thermochemical air separation and oxygen storage, J. Mater. Chem. A. 4 (2016) 13652–13659. https://doi.org/10.1039/C6TA04867F.

[5] E. Krzystowczyk, X. Wang, J. Dou, V. Haribal, F. Li, Substituted $SrFeO_3$ as robust oxygen sorbents for thermochemical air separation: correlating redox performance with compositional and structural properties, Phys. Chem. Chem. Phys. 22 (2020) 8924–8932.

https://doi.org/10.1039/d0cp00275e.

[6] A. Demizu, K. Beppu, S. Hosokawa, K. Kato, H. Asakura, K. Teramura, T. Tanaka, Oxygen storage property and chemical stability of $SrFe_{1-x}Ti_xO_{3-\delta}$ with robust perovskite structure, J. Phys. Chem. C. 121 (2017) 19358–19364. https://doi.org/10.1021/acs.jpcc.7b06078.

[7] F. Fujishiro, N. Oshima, N. Kamioka, T. Sakuragi, M. Oishi, Relationship between oxygen desorption and the reduction features of Mn and Fe in perovskite-type $SrFe_{1-x}Mn_xO_{3-\delta}$, J. Solid State Chem. 283 (2020). https://doi.org/10.1016/j.jssc.2019.121152.

[8] T. Motohashi, Y. Hirano, Y. Masubuchi, K. Oshima, T. Setoyama, S. Kikkawa, Oxygen storage capability of brownmillerite-type $Ca_2AlMnO_{5+\delta}$ and its application to oxygen enrichment, Chem. Mater. 25 (2013) 372–377. https://doi.org/10.1021/cm303156n.

[9] H. Kusaba, G. Sakai, K. Shimanoe, N. Miura, N. Yamazoe, Oxygen-sorptive and -desorptive properties of perovskite-related oxides under temperature-swing conditions for oxygen enrichment, Solid State Ionics. 152–153 (2002) 689–694. https://doi.org/10.1016/S0167-2738(02)00410-1.

[10] F. Fujishiro, M. Izaki, T. Hashimoto, Enhancement of the oxygen

desorption/absorption property of $BaFe_{1-x}In_xO_{3-\delta}$ by In substitution for Fe site, J. Am. Ceram. Soc. 101 (2018) 1696–1703. https://doi.org/10.1111/jace.15329.

[11] T. Uruga, H. Tanida, Y. Yoneda, K. Takeshita, S. Emura, M. Takahashi, M. Harada, Y. Nishihata, Y. Kubozono, T. Tanaka, T. Yamamoto, H. Maeda, O. Kamishima, Y. Takabayashi, Y. Nakata, H. Kimura, S. Goto, T. Ishikawa, The XAFS beamline BL01B1 at SPring-8, J. Synchrotron Radiat. 6 (1999) 143–145. https://doi.org/10.1107/S0909049598016173.

[12] M. Oishi, T. Sakuragi, T. Ina, N. Oshima, F. Fujishiro, In situ evaluation of the electronic/local structure in B-site mixed perovskite-type oxide $SrFe_{0.6}Mn_{0.4}O_{3-\delta}$, J. Solid State Chem. 294 (2021). https://doi.org/10.1016/j.jssc.2020.121893.

[13] B. Ravel, M. Newville, ATHENA, ARTEMIS, HEPHAESTUS: data analysis for X-ray absorption spectroscopy using IFEFFIT, J. Synchrotron Radiat. 12 (2005) 537–541. https://doi.org/10.1107/S0909049505012719.

[14] J.P. Hodges, S. Short, J.D. Jorgensen, X. Xiong, B. Dabrowski, S.M. Mini, C.W. Kimball, Evolution of oxygen-vacancy ordered crystal structures in the perovskite series $Sr_nFe_nO_{3n-1}$ ($n = 2$, 4, 8, and ∞), and the relationship to electronic and magnetic properties, J. Solid State Chem. 151 (2000) 190–209. https://doi.org/10.1006/jssc.1999.8640.

[15] R. Le Toquin, W. Paulus, A. Cousson, C. Prestipino, C. Lamberti, Time-resolved in

situ studies of oxygen intercalation into $SrCoO_{2.5}$, performed by neutron diffraction and X-ray absorption spectroscopy, J. Am. Chem. Soc. 128 (2006) 13161–13174. https://doi.org/10.1021/ja063207m.

[16] R.D. Shannon, Revised effective ionic radii and systematic studies of interatomic distances in halides and chalcogenides, Acta Cryst. A. 32 (1976) 751–767. https://doi.org/10.1107/S0567739476001551.

[17] H. Taguchi, S. Matsuoka, M. Kato, K. Hirota, Crystal structure and methane oxidation on perovskite-type $(La_{1-x}Nd_x)CoO_3$ synthesized using citric acid, J. Mater. Sci. 44 (2009) 5732–5736. https://doi.org/10.1007/s10853-009-3802-3.

[18] T. Jia, E.J. Popczun, J.W. Lekse, Y. Duan, The optimal co-doping of $SrFe_{1-x}Co_xO_{3-\delta}$ oxygen carriers in redox applications, Phys. Chem. Chem. Phys. 22 (2020) 16721–16726. https://doi.org/10.1039/d0cp02835e.

[19] J. Dou, E. Krzystowczyk, X. Wang, T. Robbins, L. Ma, X. Liu, F. Li, A- and B-site codoped $SrFeO_3$ oxygen sorbents for enhanced chemical looping air separation, ChemSusChem. 13 (2020) 385–393. https://doi.org/10.1002/cssc.201902698.

https://doi.org/10.1103/PhysRevB.45.1561.

[20] R.H. Potze, G.A. Sawatzky, M. Abbate, Possibility for an intermediate-spin ground state in the charge-transfer material $SrCoO_3$, Phys. Rev. B Condens. Matter. 51 (1995)

11501–11506. https://doi.org/10.1103/PhysRevB.51.11501.

[21] A. Maignan, C. Martin, N. Nguyen, B. Raveau, Magnetoresistance in the ferromagnetic metallic perovskite $SrFe_{1-x}Co_xO_{3-\delta}$, Solid State Sci. 3 (2001) 57–63. https://doi.org/10.1016/S1293-2558(00)01123-7.

[22] A. Muñoz, J.A. Alonso, M.J. Martínez-Lope, C. de la Calle, M.T. Fernández-Díaz, High pressure synthesis, crystal, magnetic structure and magnetotransport of $SrFe_{0.5}Co_{0.5}O_{3-\delta}$, J. Solid State Chem. 179 (2006) 3365–3370. https://doi.org/10.1016/j.jssc.2006.07.004.

[23] S. Yamaguchi, Y. Okimoto, Y. Tokura, Bandwidth dependence of insulator-metal transitions in perovskite cobalt oxides, Phys. Rev. B Condens. Matter. 54 (1996) R11022–R11025. https://doi.org/10.1103/PhysRevB.54.R11022.

[24] A.E. Bocquet, A. Fujimori, T. Mizokawa, T. Saitoh, H. Namatame, S. Suga, N. Kimizuka, Y. Takeda, M. Takano, Electronic structure of $SrFe^{4+}O_3$ and related Fe perovskite oxides, Phys. Rev. B Condens. Matter. 45 (1992) 1561–1570. https://doi.org/10.1103/physrevb.45.1561.

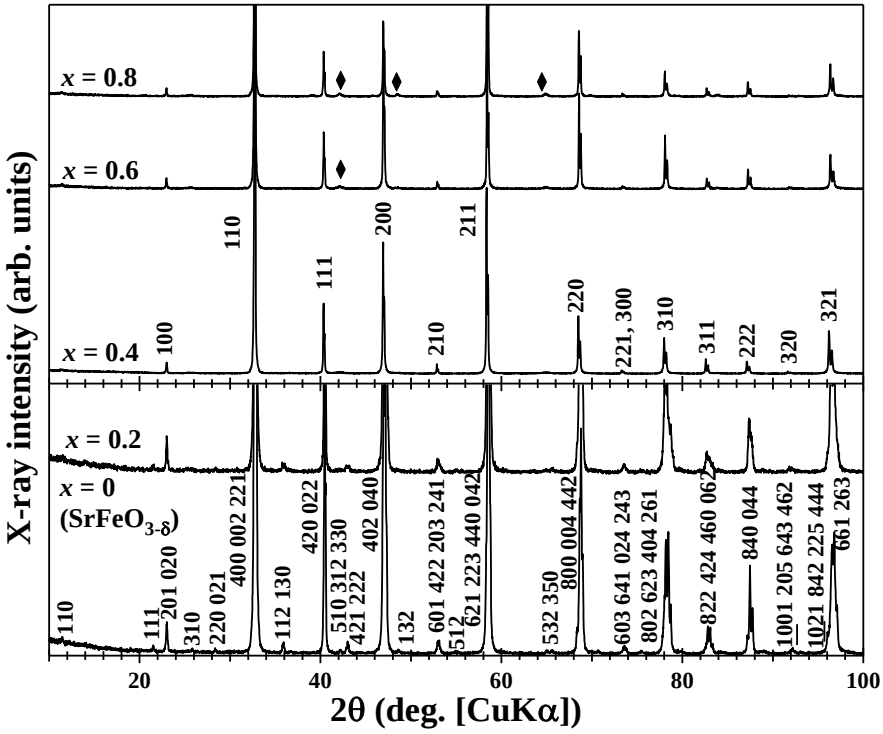

Figure 1. XRD patterns of the $SrFe_{1-x}Co_xO_{3-\delta}$ samples. Samples with $0 \leq x \leq 0.2$ were identified as an orthorhombic phase. The patterns of samples with $0.4 \leq x \leq 0.8$ were assigned to a cubic perovskite-type structure except for the peaks denoted by diamond symbols.

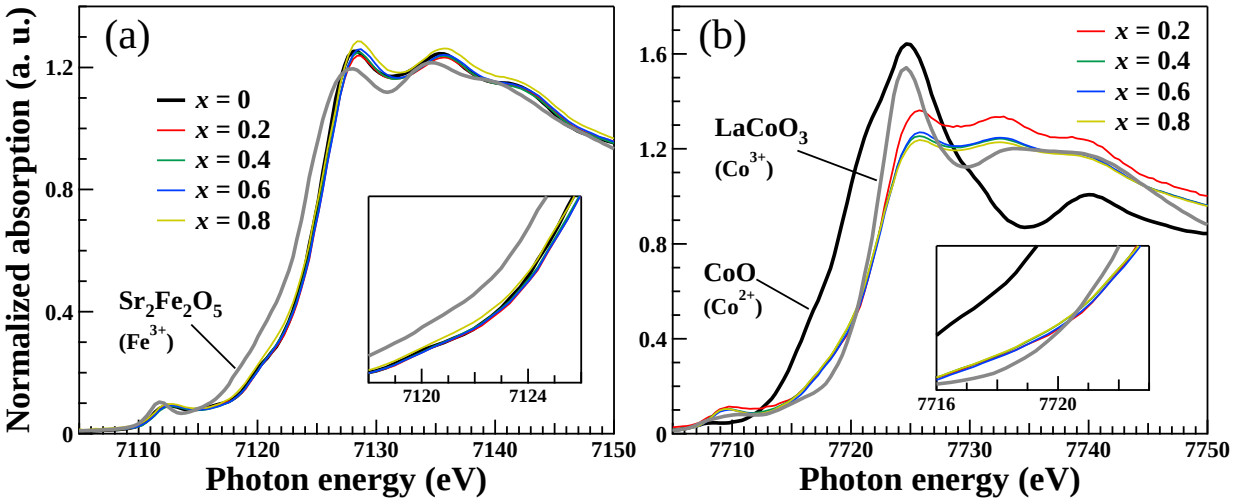

Figure 2. Normalized XANES spectra of the $SrFe_{1-x}Co_xO_{3-\delta}$ samples. (a) Fe *K*-edge spectra of all samples, and (b) Co *K*-edge spectra of samples with $0.2 \leq x \leq 0.8$. The spectra of $Sr_2Fe_2O_5$, $LaCoO_3$, and CoO are shown for reference.

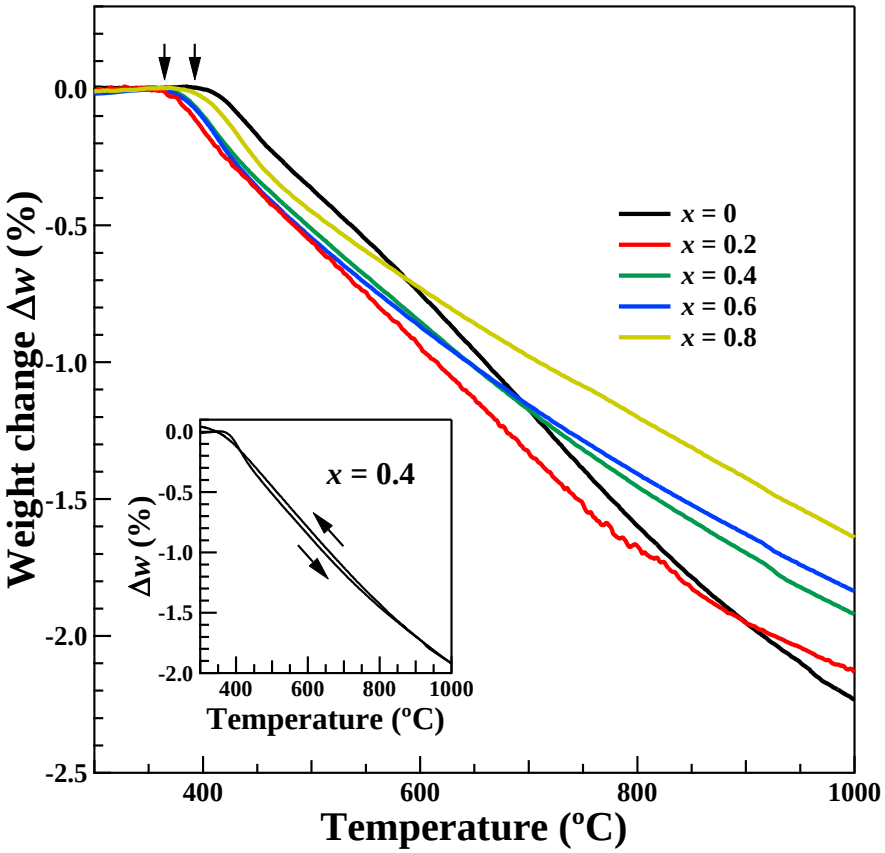

Figure 3. Weight change Δw of the $SrFe_{1-x}Co_xO_{3-\delta}$ samples in air as a function of temperature. As an example, the Δw obtained by one cycle of heating/cooling is shown for the sample with $x = 0.4$ in the inset.

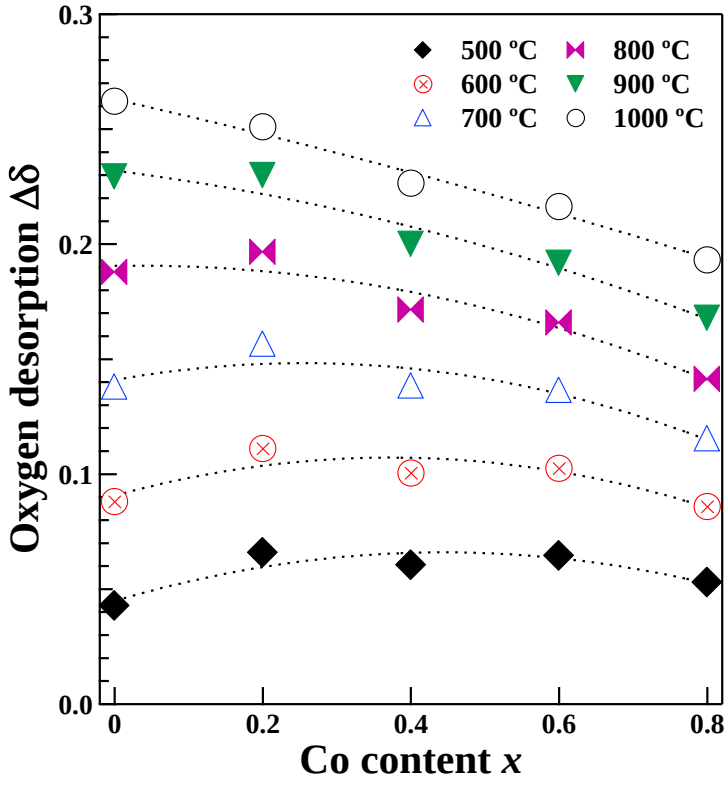

Figure 4. Amount of oxygen desorption Δδ estimated using the Δ*w* data in Fig. 3.

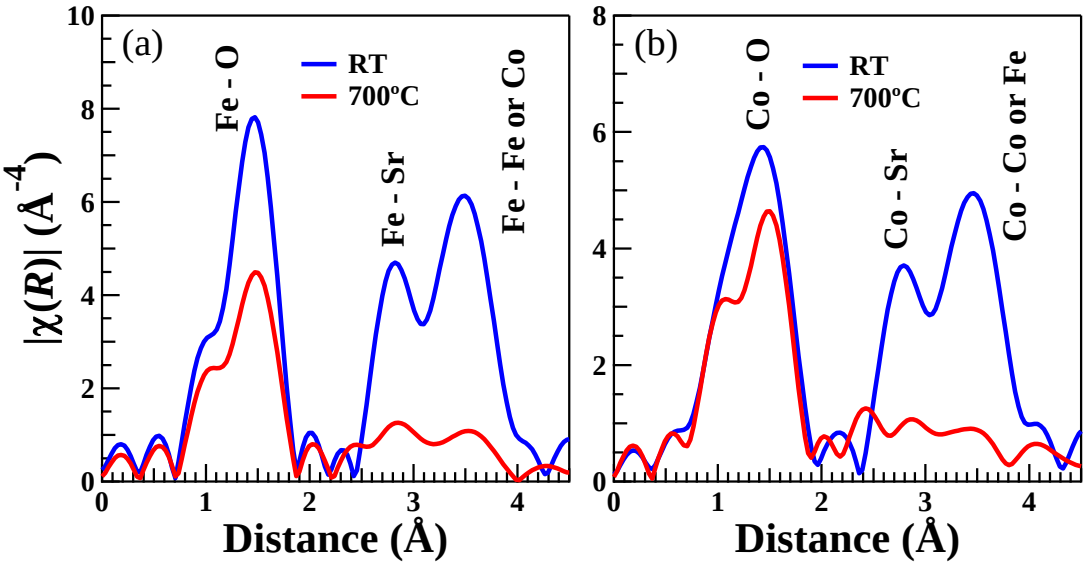

Figure 5 Amplitudes of Fourier transforms of the k^3-weighted EXAFS oscillations obtained for the $SrFe_{0.6}Co_{0.4}O_{3-\delta}$ sample at room temperature and 700 ºC. The results for Fe and Co ions are shown in (a) and (b), respectively.

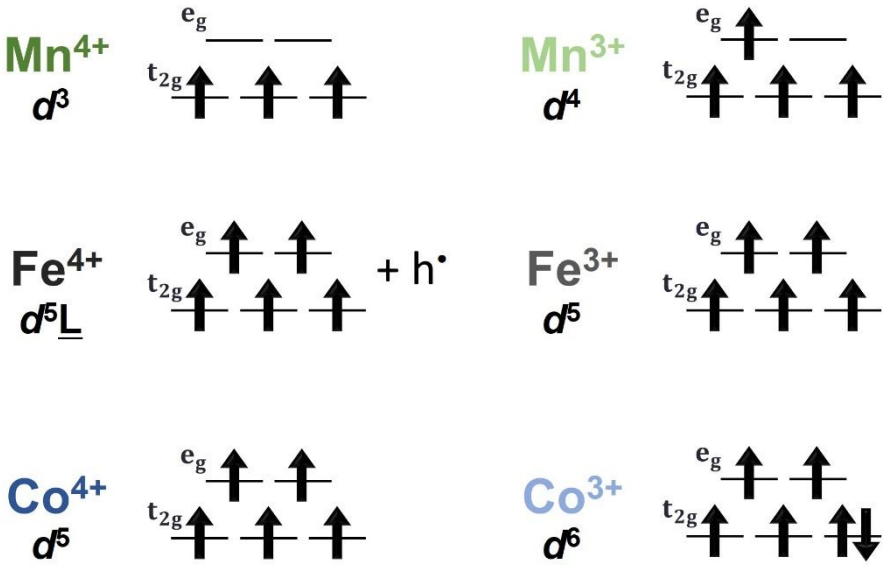

Figure 6 The electronic configurations of Mn, Fe and Co ions in the cubic perovskite-type $SrFe_{1-x}M_xO_{3-\delta}$ (M = Mn, Co). The L refers a ligand hole h•.

Table 1 Average valence of the *B*-site ions, oxygen (3−δ) and vacancy (δ) contents in the $SrFe_{1-x}Co_xO_{3-\delta}$ samples.

	Average valence of the *B*-site ions	Oxygen 3−δ	Vacancy δ	Estimated *B* valence*
$SrFeO_{3-\delta}$ ($x = 0$)[7]	3.56(2)+	2.78	0.22	-
$SrFe_{0.8}Co_{0.2}O_{3-\delta}$ ($x = 0.2$)	3.53(1)+	2.76	0.24	3.50
$SrFe_{0.6}Co_{0.4}O_{3-\delta}$ ($x = 0.4$)	3.50(1)+	2.75	0.25	3.44
$SrFe_{0.4}Co_{0.6}O_{3-\delta}$ ($x = 0.6$)	3.39(1)+	2.70	0.30	3.39
$SrFe_{0.2}Co_{0.8}O_{3-\delta}$ ($x = 0.8$)	3.32(1)+	2.66	0.34	3.33

*The Fe valence was constant at 3.56+, and the Co valence was assumed to be 3.27+.